ASC Report No. 31/2020

On the Abramov approach for the approximation of whispering gallery modes in prolate spheroids

P. Amodio, A. Arnold, T. Levitina, G. Settanni,
E.B. Weinmüller

Institute for Analysis and Scientific Computing
Vienna University of Technology — TU Wien
www.asc.tuwien.ac.at ISBN 978-3-902627-00-1

Most recent ASC Reports

30/2020 *L. Banjai, J.M. Melenk, C. Schwab*
Exponential Convergence of hp FEM for Spectral Fractional Diffusion in Polygons

29/2020 *A. Rieder, F.-J. Sayas, J.M. Melenk*
Time domain boundary integral equations and convolution quadrature for scattering by composite media

28/2020 *E. Davoli, G. Di Fratta, D. Praetorius, M. Ruggeri*
Micromagnetics of thin films in the presence of Dzyaloshinskii-Moriya interaction

27/2020 *L. Chen, E.S. Daus, A. Holzinger, and A. Jüngel*
Rigorous derivation of population cross-diffusion systems from moderately interacting particle systems

26/2020 *G. Di Fratta, A. Jüngel, D. Praetorius, and V. Slastikov*
Spin-diffusion model for micromagnetics in the limit of long times

25/2020 *G. Gantner and D. Praetorius*
Plain convergence of adaptive algorithms without exploiting reliability and efficiency

24/2020 *M. Faustmann, M. Karkulik, J.M. Melenk*
Local convergence of the FEM for the integral fractional Laplacian

23/2020 *L. Barletti, P. Holzinger, and A. Jüngel*
Quantum drift-diffusion equations for a two-dimensional electron gas with a spin-orbit

22/2020 *A. Arnold, A. Einav, B. Signorello, and T. Wöhrer*
Large time convergence of the non-homogeneous Goldstein-Taylor equation

21/2020 *P. Heid, D. Praetorius, and T.P. Wihler*
A note on energy contraction and optimal convergence of adaptive iterative linearized finite element methods

Institute for Analysis and Scientific Computing
Vienna University of Technology
Wiedner Hauptstraße 8–10
1040 Wien, Austria

E-Mail: admin@asc.tuwien.ac.at
WWW: http://www.asc.tuwien.ac.at
FAX: +43-1-58801-10196

ISBN 978-3-902627-00-1

On the Abramov approach for the approximation of whispering gallery modes in prolate spheroids

Pierluigi Amodio[a,*], Anton Arnold[b], Tatiana Levitina[c], Giuseppina Settanni[a], Ewa B. Weinmüller[b]

[a] *Dipartimento di Matematica, Università di Bari, Italy*
[b] *Institute for Analysis and Scientific Computing, Vienna University of Technology, Austria*
[c] *Institute for Computational Mathematics, Max-Planck-Institut für Sonnensystemforschung, Göttingen, Germany*

Dedicated to the memory of Aleksandr A. Abramov

Abstract

In this paper, we present the Abramov approach for the numerical simulation of the whispering gallery modes in prolate spheroids. The main idea of this approach is the Newton-Raphson technique combined with the quasi-time marching. In the first step, a solution of a simpler problem, as an initial guess for the Newton-Raphson iterations, is provided. Then, step-by-step, this simpler problem is converted into the original problem, while the quasi-time parameter τ runs from $\tau = 0$ to $\tau = 1$. While following the involved imaginary path two numerical approaches are realized, the first is based on the Prüfer angle technique, the second on high order finite difference schemes.

Keywords: Separation of variables, 'Whispering gallery' mode, multi-parameter spectral problems, Prüfer angle, High accuracy finite differences
2000 MSC: 34B09, 65L15, 65L10

1. Introduction

'A whispering gallery is usually a circular, hemispherical, elliptical or ellipsoidal enclosure, often beneath a dome or a vault, in which whispers can be heard clearly in other parts of the gallery.' Famous examples are St. Paul's Cathedral in London and the Temple of Heaven in Beijing, for more details see [30]. The involved oscillations are strongly localized within a narrow ring on the 'equator' of the resonator surface and show an extremely high quality factor (QF) [16, 24]. Especially, the high QF explains growing interest in whispering gallery modes (WGMs). This phenomenon is related to standing waves, typically described by the Helmholtz equation, which has the advantage to be separable in spheroidal coordinates [25]. It also arises in many important scientific and industrial applications in the context of optics and photonics [14, 22, 23, 24, 31].

In our earlier work, [5, 6], we discussed the numerical simulation of scalar (acoustic) eigen-oscillations inside a prolate and an oblate spheroid with a focus on WGMs. In order

*Corresponding author
Email addresses: pierluigi.amodio@uniba.it (Pierluigi Amodio), anton.arnold@tuwien.ac.at (Anton Arnold), levitina@mps.mpg.de (Tatiana Levitina), giuseppina.settanni@uniba.it (Giuseppina Settanni), e.weinmueller@tuwien.ac.at (Ewa B. Weinmüller)

to compute the eigenfunctions of the Helmholtz equation in spheroidal geometries, separation of variables simplifies the matter. There, one uses a product ansatz for the Helmholtz solution consisting of three factors. While the azimuthal contribution is explicitly known (trigonometric with m oscillations), the angular or radial solution components are described by a system of two ODEs called *prolate spheroidal wave equations*. However, the separated equations remain coupled via the separation constant and the eigenfrequency (specified by the wave number of the Helmholtz equation and the geometry). Together with the boundary conditions they constitute a singular self-adjoint two-parameter Sturm–Liouville problem.

For the above Sturm-Liouville system, we now use the general multi-parameter spectral theory to show the existence of a two-parameter eigenvalue and an associated two-component eigenfunction. They depend on a multi-index (l, n), where l and n are two non-negative integers which indicate the number of oscillations of the two eigenfunction components in angular and radial directions, respectively, [26, 27, 28]. In the framework of factored solutions, one can single out WGMs from the entire variety of oscillations occurring inside a spheroid in terms of the multi-index (l, n) and the azimuthal number m. Typically, WGMs correspond to small indices $l, n \sim 0-50$, and very large azimuthal numbers $m \sim 100-10.000$.

Singular Sturm–Liouville problems are difficult to deal with numerically, solution and direction fields are in general unbounded, and therefore, they require specific techniques. In [5, 6], we offered two alternative techniques one of which was based on the Prüfer angle properties, while the other one was based on high order finite difference schemes. Although these techniques allowed evaluation of the eigenmodes of a spheroidal resonator in a wide range of parameters, they could not cover the whole spectrum of parameters important for practical applications. In particular, WGM calculations inside extremely prolate spheroids were not possible. Moreover, neither one of the approaches [5, 6] could be converted into an automatic procedure and had to be controlled manually. On the one hand, the approach based on the Prüfer transformation required special monotonicity of spectral curves expressing mutual dependencies of spectral parameters in separated equations. Otherwise one had to find a linear combination of spectral parameters that would provide the required monotonicity. The success of the application, especially the convergence rate, strongly depends on the choice of such a transformation. On the other hand, the difficulty in applying the high accuracy schemes to solve the underlying nonlinear problem was to provide appropriately accurate starting values of the eigenparameters.

Also, the generalization of the techniques [5, 6] to a larger number of spectral parameters seems not an easy task.

The objective of the present work is to develop a technique for numerically solving singular multi–parameter spectral problems free from the above-mentioned deficiencies and to weaken the restrictions on the parameters of the WGM calculations in prolate spheroids. To this end, we shall utilize results outlined by Abramov and co-authors in [3, 4].

The algorithm given in [3] for solving regular multi-parameter Sturm-Liouville problems is applicable for any number of spectral parameters and in regular cases does not require manual control. Moreover, in the later paper [4] the question how to extend the results of [3] to the singular case was discussed. The theoretical prediction for the convergence, stability and tolerance given in [4] fails for such extreme cases as WGM mode evaluation: The gradients of functions implicitly used in the estimates in [3, 4] become too large to directly apply the Abramov algorithm. Furthermore, the boundary conditions imposed at singular points require a more careful treatment than the one recommended in [4].

The basis of Abramov's approach is the Newton-Raphson technique assembled with the quasi-time marching. One begins with a solution of a simpler problem as an initial guess for the Newton-Raphson iterations; this corresponds to the quasi-time parameter $\tau = 0$. Then,

step-by-step, this simpler problem is converted into the original problem, as the quasi-time parameter τ increases in the interval $\tau \in [0, 1]$. This idea is the basis for both numerical approaches discussed hereafter and is combined with the advantageous features of techniques [5, 6].

The structure of the paper is as follows. In the next section, we give a short survey over the spheroidal coordinates and prolate spheroidal wave functions (PSWF). In Section 3, the Prüfer angles associated with the angular and radial PSWF are introduced to give an equivalent algebraic formulation of the two-parameter Sturm–Liouville problem. The Abramov method is briefly described in Section 4. In Section 5, we discuss in the context of the Abramov method, the transfer of the boundary condition posed at the singular point to a close regular point. The application of the modified Abramov method for the WGM calculations is considered in Section 6. Section 7 is devoted to the finite difference schemes combined with parameter marching. In Section 8, the related numerical simulation results are presented and compared.

2. Prolate spheroidal coordinates and prolate spheroidal wave functions

A thorough description of spheroidal coordinates and the related separation of variables can be found in [25, 18]. For more details we additionally refer the reader to our recent paper [7]. Below, we only provide information required for the further considerations keeping the notations introduced in [7].

Provided that, on the surface of the spheroidal resonator ($\mathcal{S}$) either Dirichlet or Neumann boundary condition is imposed and due to the rotational symmetry around the z-axis, the 3D simulation of the eigen oscillations inside this resonator reduces to the two–parameter singular self–adjoint Sturm–Liouville (SL) problem with respect to the separation constant λ and the squared dimensionless wave number c. The SL-problem is defined [18, 29] by the ODEs coupled through λ and c^2,

$$\frac{d}{d\eta}(1-\eta^2)\frac{d}{d\eta}S + Q_a(\eta,\lambda,c^2)\,S \;=\; 0, \quad -1<\eta<1, \tag{1}$$

$$\frac{d}{d\xi}(\xi^2-1)\frac{d}{d\xi}R + Q_r(\xi,\lambda,c^2)\,R \;=\; 0, \qquad 1<\xi<\xi_s, \tag{2}$$

with

$$\begin{aligned} Q_a(\eta,\lambda,c^2) &= \lambda + c^2(1-\eta^2) - \frac{m^2}{1-\eta^2}, \\ Q_r(\xi,\lambda,c^2) &= c^2(\xi^2-1) - \lambda - \frac{m^2}{\xi^2-1}. \end{aligned}$$

Moreover, we require the solutions of these equations to be bounded in the neighbourhood of the singular points $\eta = \pm 1$, $\xi = 1$, and to satisfy either one of the following terminal conditions

$$R(\xi_s) = 0, \quad R'(\xi_s) = 0, \tag{3}$$

in a correspondence with the boundary condition, Dirichlet or Neumann, imposed on the surface $\mathcal{S}$.

Above, η and ξ denote the angular and radial coordinates on an arbitrary z–w plane with fixed polar angle $\varphi = \varphi_0$. They relate to the Cartesian coordinates z and w as

$$w = \frac{d}{2}\sqrt{(\xi^2-1)(1-\eta^2)}, \quad z = \frac{d}{2}\xi\eta,$$

with d being the resonator focal length. The conventional coordinates x, y are here

$$x = w\cos\varphi_0, \quad y = w\sin\varphi_0.$$

By $\xi = \xi_s$ we denote the radial coordinate describing the resonator surface $\mathcal{S}$.

The number m in the right-hand sides of Eqs. (1), (2) is the azimuthal index, $m = 0, 1, 2, \ldots$. The case $m = 0$ plays no role in the simulation of the 'whispering gallery' phenomenon and will be omitted hereafter.

The angular equation (1) is invariant with respect to the replacement $\eta \to -\eta$. As a consequence its solutions bounded at both ends of the interval $(-1, 1)$ are either odd or even, which allows one to consider Eq. (1) on the half-interval $[0, 1)$ taking the 'parity' boundary condition at $\eta = 0$ into account, i.e.

$$\text{either } S(0) = 0 \quad \text{or} \quad S'(0) = 0. \tag{4}$$

Let $\beta_a(\eta)$, $\beta_r(\xi)$ be the modified logarithmic derivatives of $S(\eta)$ and $R(\xi)$,

$$\beta_a(\eta) = (1-\eta^2)S'(\eta)/S(\eta) \quad \text{and} \quad \beta_r(\xi) = (\xi^2-1)R'(\xi)/R(\xi).$$

These auxiliary functions, $\beta_a(\eta)$, $\beta_r(\xi)$, allow to reformulate the boundedness conditions. Let $m > 0$, then any solution of Eq. (1) (Eq. (2)) bounded at $\eta = 1$ ($\xi = 1$), satisfies

$$\lim_{\eta\to 1_{-0}} \beta_a(\eta) = -m, \quad \lim_{\xi\to 1_{+0}} \beta_r(\xi) = m. \tag{5}$$

For the proof, see e.g. [1, 21].

The solution of the problem (1)–(5) is not uniquely defined. To make it unique we fix the multi–index (l, n), i.e. the numbers of internal zeros l, n, that the angular and radial components $S(\eta)$ and $R(\xi)$ possess inside the intervals $(-1, 1)$ and $(1, \xi_s)$. It is the parity of the index l that defines the parity of the angular function S_{ln}. In other words, it defines the choice of the boundary conditions in (4).

We also require that

$$\int_{-1}^{1} S_{ln}^2(\eta)\, d\eta \;=\; 1, \quad \int_{1}^{\xi_s} R_{ln}^2(\xi)\, d\xi \;=\; 1. \tag{6}$$

In the next section the logarithmic derivatives, $\beta_a(\eta)$, $\beta_r(\xi)$, along with the related Prüfer angles defined by Eq. (9) will be used to reformulate the problem (1)–(5) into a form which is more suitable for the quasi-time marching and Newton's method application. The solvability of the problem (1)–(5), as well as the solvability of the intermediate problems arising in the course of calculation, follow from the general multi-parameter spectral theory [13, 27, 28].

3. Logarithmic derivative, Prüfer angle and the equivalent algebraic problem

In the sequel, the multi-index (l, n) and the azimuthal number $m > 0$ are fixed, as well as the boundary condition (3) on the surface of the resonator $\mathcal{S}$. In what follows the multi-index (l, n) is omitted in case this does not cause a confusion.

Given arbitrary λ, c^2, the logarithmic derivatives $\beta_a(\eta)$, $\beta_r(\xi)$ satisfy the Riccati equations

$$\beta_a' + \frac{\beta_a^2}{1-\eta^2} + Q_a(\eta) = 0, \qquad \eta \in (0, 1), \tag{7}$$

$$\beta_r' + \frac{\beta_r^2}{\xi^2-1} + Q_r(\xi) = 0, \qquad \xi \in (1, \xi_s), \tag{8}$$

everywhere, except at the nodes of the associated functions $S(\eta, \lambda, c^2)$ and $R(\xi, \lambda, c^2)$ where $\beta_a(\eta)$, $\beta_r(\xi)$ blow up to $\pm\infty$.

Let us introduce the Prüfer angles $\theta_a(\eta)$ and $\theta_r(\xi)$ related to the solutions of Eqs. (1)–(2), respectively, which are bounded at the singular points $\eta = 1$ and $\xi = 1$. Consider solutions to the nonlinear ODEs,

$$\begin{aligned} {\theta_a}' &= \frac{\sin^2(\theta_a)}{(1-\eta^2)} + Q_a(\eta)\cos^2(\theta_a) \quad \eta \in (0,1), \\ {\theta_r}' &= \frac{\sin^2(\theta_r)}{(\xi^2-1)} + Q_r(\xi)\cos^2(\theta_r), \quad \xi \in (1,\xi_s), \end{aligned} \tag{9}$$

subject to the initial conditions

$$\lim_{\eta \to 1_{-0}} \theta_a(\eta) = \arctan m, \tag{10}$$

and

$$\lim_{\xi \to 1_{+0}} \theta_r(\xi) = -\arctan m, \tag{11}$$

respectively.

A direct substitution into Eqs. (7) and (8) shows that $\tan\theta_a(\eta) = -\beta_a(\eta)$ and $\tan\theta_r(\xi) = -\beta_r(\xi)$, while the initial conditions (3) and (4) imply requirements (5). Unlike the logarithmic derivatives $\beta_a(\eta)$ and $\beta_r(\xi)$, their Prüfer angles remain continuous over the intervals $(0,1)$ and $(1,\xi_s)$.

We consider now solutions of Eq. (1) satisfying the boundary condition (4). Their corresponding Prüfer angle at $\eta = 0$, i.e. $\theta_a(0)$, is defined up to a multiple of π by either 0 or $\pi/2$, depending on the parity of index l. The boundary condition (3) implies in the Dirichlet case $\theta_r(\xi_s) = \pi/2$, while in the Neumann case $\theta_r(\xi_s) = 0$, as above, up to a multiple of π.

Each time when either $S(\eta, \lambda, c^2) = 0$ or $R(\xi, \lambda, c^2) = 0$, the associated Prüfer angle $\theta_a(\eta)$ or $\theta_r(\xi)$ crosses a horizontal $\theta = k\pi + \dfrac{\pi}{2}$, $k \in \mathbb{N}$ and vice versa. Although both $\theta_a(\eta)$ and $\theta_r(\xi)$ are not monotone, they increase at the points where the functions $S(\eta, \lambda, c^2)$, $R(\xi, \lambda, c^2)$ vanish, see (9). Thus θ_a and θ_r reckon up the nodes that the related solutions have within their definition intervals.

Summarizing the above, we obtain an algebraic problem equivalent to the original Sturm–Liouville problem: Denote

$$\begin{aligned} \varphi_a(\lambda, c^2) &:= -\frac{l\pi}{2} - \theta_a(0), \\ \varphi_r(\lambda, c^2) &:= \theta_r(\xi_s) - \begin{cases} n\pi, & \text{for the Neumann condition (3),} \\ \left(n + \dfrac{1}{2}\right)\pi, & \text{for the Dirichlet condition (3).} \end{cases} \end{aligned}$$

Then, the point (λ, c^2) is the desired eigenvalue of the multi-index (l, n) iff

$$\varphi_a(\lambda, c^2) = \varphi_r(\lambda, c^2) = 0. \tag{12}$$

4. Abramov approach

In this section, we give a quick overview of the ideas behind the Abramov method.

As an initial step, the factors $(1-\eta^2)$ and (ξ^2-1) standing in Eqs. (1), (2) after the eigenvalue component c^2 are 'frozen' at an arbitrary point $(\eta_f, \xi_f) \in (0,1)\times(1,\xi_s)$. Although the 'frozen' problem

$$\frac{d}{d\eta}(1-\eta^2)\frac{d}{d\eta}S \quad + \quad \left[\lambda + c^2(1-\eta_f^2) - \frac{m^2}{1-\eta^2}\right] S = 0, \quad 0<\eta<1, \tag{13}$$

$$\frac{d}{d\xi}(\xi^2-1)\frac{d}{d\xi}R \quad + \quad \left[c^2(\xi_f^2-1) - \lambda - \frac{m^2}{\xi^2-1}\right] R = 0, \quad 1<\xi<\xi_s, \tag{14}$$

remains formally two–parameter, each equation may be considered independently with respect to the eigenparameters

$$\mu = \lambda + c^2(1-\eta_f^2), \quad \nu = c^2(\xi_f^2-1) - \lambda.$$

For the numerical solution of problems similar to (13), (4), (5) and (14), (3), (5) we refer the reader, e.g. to [1, 9, 10, 21].

The parameters λ and c^2 are expressed through $\mu = \mu_l$ and $\nu = \nu_n$ as follows:

$$\begin{pmatrix} \lambda_f \\ c_f^2 \end{pmatrix} = \frac{1}{\xi_f^2 - \eta_f^2} \begin{pmatrix} \xi_f^2 - 1 & \eta_f^2 - 1 \\ 1 & 1 \end{pmatrix} \begin{pmatrix} \mu_l \\ \nu_n \end{pmatrix}. \tag{15}$$

The values λ_f, c_f^2 are used as starting guesses for the marching procedure, i.e. we define

$$\lambda_0 = \lambda_f, \quad c_0^2 = c_f^2. \tag{16}$$

Let

$$0 = \tau_0 \le \tau_1 \le \ldots \le \tau_p \le \ldots \le \tau_P = 1 \tag{17}$$

and replace Q_a and Q_r in Eqs. (1) and (2) by

$$\begin{aligned} Q_{ap}(\eta,\lambda,c^2) &= \lambda + c^2\left[(1-\eta_f^2)(1-\tau_p) + (1-\eta^2)\tau_p\right] - \frac{m^2}{1-\eta^2}, \\ Q_{rp}(\xi,\lambda,c^2) &= c^2\left[(\xi_f^2-1)(1-\tau_p) + (\xi^2-1)\tau_p\right] - \lambda - \frac{m^2}{\xi^2-1}. \end{aligned}$$

Then, in the p-th step the problem is defined by

$$\frac{d}{d\eta}(1-\eta^2)\frac{d}{d\eta}S_p \quad + \quad Q_{ap}(\eta,\lambda,c^2)\, S_p = 0, \quad 0<\eta<1, \tag{18}$$

$$\frac{d}{d\xi}(\xi^2-1)\frac{d}{d\xi}R_p \quad + \quad Q_{rp}(\xi,\lambda,c^2) R_p = 0, \quad 1<\xi<\xi_s. \tag{19}$$

Note that the quasi-time parameter τ changing over the interval $[0,1]$ allows a gradual transition from the problem (13)–(14) with 'frozen' coefficients (for $\tau = 0$) to the original problem defined by Eqs. (1)–(2) (for $\tau = 1$).

The boundary conditions (4) and (3) are now posed for S_p and R_p, respectively. According to the parity of index l either $S_p(0) = 0$ or $S_p'(0) = 0$ holds. For the radial function R_p, we require either $R_p(\xi_s) = 0$ or $R_p'(\xi_s) = 0$ to hold, depending on the boundary conditions imposed on the surface of the spheroid $\mathcal{S}$. Moreover,

$$\beta_{ap}(\eta) = (1-\eta^2)S_p'(\eta)/S_p(\eta) \to -m, \quad \text{as } \eta \to 1_{-0}, \tag{20}$$

$$\beta_{rp}(\xi) = (\xi^2-1)R_p'(\xi)/R_p(\xi) \to m, \quad \text{as } \xi \to 1_{+0}. \tag{21}$$

The p-th approximation to the eigenparameters, λ_p, c_p^2, $p = 1, 2, \ldots, P$, is computed as one Newton iteration step for the above p-th problem,

$$\left(\begin{array}{c} \lambda_p \\ c_p^2 \end{array} \right) = \left(\begin{array}{c} \lambda_{p-1} \\ c_{p-1}^2 \end{array} \right) - \Psi_p^{-1} \times \left(\begin{array}{c} \varphi_{ap}(\lambda_{p-1}, c_{p-1}^2) \\ \varphi_{rp}(\lambda_{p-1}, c_{p-1}^2) \end{array} \right). \tag{22}$$

Here, the discrepancy functions $\varphi_{ap}(\lambda, c^2)$ and $\varphi_{rp}(\lambda, c^2)$ are defined similar to $\varphi_a(\lambda, c^2)$ and $\varphi_r(\lambda, c^2)$,

$$\begin{aligned} \varphi_{ap}(\lambda, c^2) &= -\frac{l\pi}{2} - \theta_{ap}(0), \\ \varphi_{rp}(\lambda, c^2) &= \theta_{rp}(\xi_s) - \left\{ \begin{array}{ll} n\pi, & \text{for the Neumann condition (3)}, \\ \left(n + \dfrac{1}{2}\right)\pi, & \text{for the Dirichlet condition (3)}, \end{array} \right. \end{aligned} \tag{23}$$

and the Jacobi matrix Ψ_p is

$$\Psi_p = \left(\begin{array}{cc} \Psi_{p11} & \Psi_{p12} \\ \Psi_{p21} & \Psi_{p22} \end{array} \right) = \left(\begin{array}{cc} \dfrac{\partial \varphi_{ap}}{\partial \lambda} & \dfrac{\partial \varphi_{ap}}{\partial c^2} \\ \dfrac{\partial \varphi_{rp}}{\partial \lambda} & \dfrac{\partial \varphi_{rp}}{\partial c^2} \end{array} \right)_{\substack{\lambda = \lambda_{p-1} \\ c^2 = c_{p-1}^2}}.$$

As before, the Prüfer angles $\theta_{ap}(\eta)$ and $\theta_{rp}(\xi)$ correspond to the bounded solutions of Eqs. (18), (19). Since

$$\beta_{ap}' + \frac{\beta_{ap}^2}{1 - \eta^2} + Q_{ap}(\eta) = 0, \qquad \eta \in (0, 1), \tag{24}$$

$$\beta_{rp}' + \frac{\beta_{rp}^2}{\xi^2 - 1} + Q_{rp}(\xi) = 0, \qquad \xi \in (1, \xi_s), \tag{25}$$

and due to the relations (20), (21), the functions $\theta_{ap}(\eta)$ and $\theta_{rp}(\xi)$ satisfy the equations

$$\frac{\partial \theta_{ap}}{\partial \eta} = \frac{\sin^2(\theta_{ap})}{(1 - \eta^2)} + Q_{ap}(\eta, \lambda, c^2)\cos^2(\theta_{ap}), \quad 0 \le \eta < 1, \tag{26}$$

$$\frac{\partial \theta_{rp}}{\partial \xi} = \frac{\sin^2(\theta_{rp})}{(\xi^2 - 1)} + Q_{rp}(\xi, \lambda, c^2)\cos^2(\theta_{rp}), \quad 1 < \xi \le \xi_s, \tag{27}$$

as well as the conditions

$$\lim_{\eta \to 1_{-0}} \theta_{ap}(\eta) = \arctan(m), \quad \lim_{\xi \to 1_{+0}} \theta_{rp}(\xi) = -\arctan(m). \tag{28}$$

Taking derivatives of Eqs. (26)–(27) with respect to λ and c^2, the entries of the Jacobi

matrix Ψ_p are expressed through the solutions of the equations

$$\begin{aligned}
\frac{\partial \kappa_{11}}{\partial \eta} &= 2\sin\theta_{ap}\cos\theta_{ap}\left[Q_{ap}(\eta,\lambda,c^2)+\frac{1}{1-\eta^2}\right]\kappa_{11}+\cos^2\theta_{ap},\\
\frac{\partial \kappa_{12}}{\partial \eta} &= 2\sin\theta_{ap}\cos\theta_{ap}\left[Q_{ap}(\eta,\lambda,c^2)+\frac{1}{1-\eta^2}\right]\kappa_{12}\\
&\quad+\left[(1-\eta_f^2)(1-\tau)+(1-\eta^2)\tau\right]\cos^2\theta_{ap},\\
\frac{\partial \kappa_{21}}{\partial \xi} &= 2\sin\theta_{rp}\cos\theta_{rp}\left[Q_{rp}(\xi,\lambda,c^2)+\frac{1}{\xi^2-1}\right]\kappa_{21}-\cos^2\theta_{rp},\\
\frac{\partial \kappa_{22}}{\partial \xi} &= 2\sin\theta_{rp}\cos\theta_{rp}\left[Q_{rp}(\xi,\lambda,c^2)+\frac{1}{\xi^2-1}\right]\kappa_{22}\\
&\quad+\left[(\xi_f^2-1)(1-\tau)+(\xi^2-1)\tau\right]\cos^2\theta_{rp}.
\end{aligned} \tag{29}$$

Conditions (28) yield

$$\lim_{\eta\to 1_{-0}}\kappa_{11}(\eta)=\lim_{\eta\to 1_{-0}}\kappa_{12}(\eta)=\lim_{\xi\to 1_{+0}}\kappa_{21}(\xi)=\lim_{\xi\to 1_{+0}}\kappa_{22}(\xi)=0. \tag{30}$$

The functions κ_{ij} are integrated together with Eqs. (26)–(27) over the intervals $(0,1)$ and $(1,\xi_s)$. Taking (23) into account, we obtain

$$\Psi_p=\begin{pmatrix}\kappa_{11}(0) & \kappa_{12}(0)\\ \kappa_{21}(\xi_s) & \kappa_{22}(\xi_s)\end{pmatrix}.$$

The analysis presented in [3, 4] applies to the problem (1)–(5). Thus, for any $p=1,2,\ldots,P$ the following assertions hold:

- For any multi-index (l,n) the p-th problem defined by Eqs. (18)–(19) is solvable. We denote by $(\lambda(\tau_p),c^2(\tau_p))$ its exact eigenvalue;
- Inside the rectangle $[0,1)\times(1,\xi_s]$ the determinant of the matrix

  $$\det\begin{pmatrix}1 & (1-\eta^2)\\ -1 & (\xi^2-1)\end{pmatrix}=\xi^2-\eta^2>0,$$

  which guarantees that the Jacobi matrix Ψ_p, $p=0,1,\ldots,P$, remains non singular. For the proof, see [3]. The regularity of the matrix Ψ_p allows the calculation of the values λ_p, c_p^2 from (22);
- The values λ_p, c_p^2 differ from the exact eigenvalues $\lambda(\tau_p)$, $c^2(\tau_p)$ by at most Ch_τ^2, where $h_\tau=\max(\tau_p-\tau_{p-1})$, $p=1,2,\ldots,P$, is the maximal marching stepsize and the constant C does not depend on the partition $\{\tau_p\}_{p=0,1\ldots,P}$.

In practice, the direct application of the above numerical method to the problem (1)–(5), especially in case of the WGM calculations, can fail. In the next two sections, we modify the Abramov technique in order to apply it to the problem at hand. The proposed modifications are strongly in spirit of the earlier Abramov papers [1, 2].

5. Boundary conditions transfer to a regular point

The accurate integration of the auxiliary ODEs (26), (27), and (29) near singular points involves obvious difficulties. To avoid them, we transfer the conditions stated at $\eta=1$,

$\xi = 1$ to close regular points adopting the procedure specified in [1] (see also [7, 21]). For any p, $p = 0, 1, \ldots, P$, equations (18), and (19) are treated similarly.

Let $\eta_b = 1 - \delta_\eta$ and $\xi_b = 1 + \delta_\xi$, with $\delta_\eta, \delta_\xi > 0$. For fixed p, λ and c^2 all solutions of Eq. (18) (or Eq. (19)) bounded at $\eta = 1$ (at $\xi = 1$) possess the same logarithmic derivative $\beta_{ap}(\eta)$ ($\beta_{rp}(\xi)$) defined by the condition (20) (or (21)). Therefore, functions $\beta_{ap}(\eta)$ ($\beta_{rp}(\xi)$) evolving according to Eqs. (24)–(25) and satisfying the initial conditions (20) and (21) transfer the requirements for the solutions of Eqs. (18)–(19) to stay bounded on $[0, 1)$ and $(1, \xi_s]$, respectively. In particular, at $\eta = \eta_b$, $\xi = \xi_b$ the latter boundedness requirements are equivalent to the equations

$$\begin{aligned}(1 - \eta_b^2) S_p'(\eta_b) &= \beta_{ap}(\eta_b)\, S_p(\eta_b),\\ (\xi_b^2 - 1) R_p'(\xi_b) &= \beta_{rp}(\xi_b)\, R_p(\xi_b).\end{aligned}$$

In the vicinity of $\eta = 1$, the following expansion holds:

$$\beta_{ap}(\eta) = \sum_{k=0}^{\infty} \beta_{ap\,k} (1 - \eta)^k. \tag{31}$$

The coefficients $\beta_{ap\,k}$ are obtained from the Riccati equation (24) taking (20) into account. Denote $\rho_{ap} = \lambda_p + c_p^2(1 - \tau_p)(1 - \eta_f^2)$, then

$$\begin{aligned}\beta_{ap\,0} &= -m,\\ \beta_{ap\,1} &= \frac{\rho_{ap}}{1 + m},\\ \beta_{ap\,2} &= \frac{\beta_{ap\,1} - \rho_{ap} + \beta_{ap\,1}^2 + 4c_p^2\tau_p}{2\,(2 + m)},\\ \beta_{ap\,3} &= \frac{\beta_{ap\,2} - 2c_p^2\tau_p + \beta_{ap\,1}\beta_{ap\,2}}{(3 + m)},\\ \beta_{ap\,4} &= \frac{3\beta_{ap\,3} + c_p^2\tau_p + 2\beta_{ap\,1}\beta_{ap\,3} + \beta_{ap\,2}^2}{2\,(4 + m)},\\ \beta_{ap\,k} &= \frac{(k-1)\beta_{ap\,k-1} + \sum_{s=1}^{k-1} \beta_{ap\,s}\beta_{ap\,k-s}}{2\,(k + m)}, k = 5, 6, \ldots\ .\end{aligned}$$

Also, denote $\rho_{rp} = c_p^2(1 - \tau_p)(\xi_f^2 - 1) - \lambda_p$. Substituting the expansion

$$\beta_{rp}(\xi) = \sum_{k=0}^{\infty} \beta_{rp\,k} (\xi - 1)^k \tag{32}$$

into Eq. (25) yields together with (21) the coefficients $\beta_{rp\,k}$,

$$\begin{aligned}
\beta_{rp\,0} &= m,\\
\beta_{rp\,1} &= -\frac{\rho_{rp}}{1+m},\\
\beta_{rp\,2} &= -\frac{\beta_{rp\,1}+\rho_{rp}+\beta_{rp\,1}^2+4c_p^2\tau_p}{2\,(2+m)},\\
\beta_{rp\,3} &= -\frac{\beta_{rp\,2}+2c_p^2\tau_p+\beta_{rp\,1}\beta_{rp\,2}}{(3+m)},\\
\beta_{rp\,4} &= -\frac{3\beta_{rp\,3}+c_p^2\tau_p+2\beta_{rp\,1}\beta_{rp\,3}+\beta_{rp\,2}^2}{2\,(4+m)},\\
\beta_{rp\,k} &= -\frac{(k-1)\beta_{rp\,k-1}+\sum\limits_{s=1}^{k-1}\beta_{rp\,s}\beta_{rp\,k-s}}{2\,(k+m)}, k=5,6,\dots\ .
\end{aligned}$$

In [1, 21], for the case $\tau = 1$, the convergence radii σ_a and σ_r as well as the upper bound on the truncation errors in the series (31) and (32) are provided. The related analysis from [1, 21] is also applicable to an arbitrary τ_p.

Let $\mathcal{B}_{a(r)p} = \max\left\{\sqrt[k]{\left|\beta_{a(r)p\,k}\right|},\ k=1,2,3,4,5\right\}$. The series (31) and (32) are absolutely and uniformly convergent, provided that

$$\upsilon_{ap} = \mathcal{B}_{ap}\,(1-\eta) < 1 \quad \text{and} \quad \upsilon_{ar} = \mathcal{B}_{rp}\,(\xi-1) < 1.$$

The convergence is a direct consequence of the fact that the inequalities $\sqrt[k]{\left|\beta_{a(r)p\,k}\right|} \le \mathcal{B}_{a(r)p}$ hold then also for all remaining series coefficients, see [21] for details.

On the intervals of absolute convergence, series (31) and (32) can be differentiated which justifies the above calculations of the coefficients $\beta_{ap\,k}$ and $\beta_{rp\,k}$. In the calculations, we replace the boundedness conditions at the singular points by the approximate regular boundary conditions,

$$(1-\eta_b^2)S_p'(\eta_b) = \hat{\beta}_{ap}(\eta_b)\,S_p(\eta_b), \tag{33}$$

$$(\xi_b^2-1)R_p'(\xi_b) = \hat{\beta}_{rp}(\xi_b)\,R_p(\xi_b). \tag{34}$$

Here, $\hat{\beta}_{ap}$, $\hat{\beta}_{rp}$ stand for the series (31) and (32) truncated in a proper way to satisfy the desired tolerance requirement. The upper bound for the truncation error ε_N is given by the inequalities

$$\varepsilon_N \le \frac{\upsilon_{a(r)p}^{N+1}}{1-\upsilon_{a(r)p}},$$

where N is the number of terms in the truncated series [21]. For the associated Prüfer angles we obtain

$$\theta_{ap}(\eta_b) = -\arctan\hat{\beta}_{ap}(\eta_b), \quad \theta_{rp}(\xi_b) = -\arctan\hat{\beta}_{rp}(\xi_b). \tag{35}$$

In the neighbourhood of the points η_b and ξ_b, in the convergence intervals of the series (31) and (32), one can differentiate them term by term with respect to λ and c^2. Thus, for

the functions κ_{ij} the following representations[1]hold:

$$\begin{aligned}
\kappa_{1j}(\eta) &= -\sum_{k=1}^{\infty}\gamma_{1j}^{(k)}(1-\eta)^k/\left(1+\beta_{ap}^2(\eta)\right), \\
\kappa_{2j}(\xi) &= -\sum_{k=1}^{\infty}\gamma_{2j}^{(k)}(\xi-1)^k/\left(1+\beta_{rp}^2(\xi)\right), \quad j=1,2,
\end{aligned} \tag{36}$$

with the coefficients $\gamma_{ij}^{(k)}$ given by

$$\begin{aligned}
\gamma_{11}^{(1)} &= \frac{1}{1+m}, \\
\gamma_{11}^{(2)} &= \frac{\gamma_{11}^{(1)}-1+2\beta_{ap\,1}\gamma_{11}^{(1)}}{2\,(2+m)}, \\
\gamma_{11}^{(3)} &= \frac{\gamma_{11}^{(2)}+\beta_{ap\,1}\gamma_{11}^{(2)}+\beta_{ap\,2}\gamma_{11}^{(1)}}{(3+m)}, \\
\gamma_{11}^{(4)} &= \frac{3\gamma_{11}^{(3)}+2\beta_{ap\,1}\gamma_{11}^{(3)}+2\beta_{ap\,2}\gamma_{11}^{(2)}+2\beta_{ap\,3}\gamma_{11}^{(1)}}{2\,(4+m)},
\end{aligned}$$

$$\begin{aligned}
\gamma_{12}^{(1)} &= \frac{(1-\tau_p)(1-\eta_f^2)}{1+m}, \\
\gamma_{12}^{(2)} &= \frac{\gamma_{12}^{(1)}-(1-\tau_p)(1-\eta_f^2)+2\beta_{ap\,1}\gamma_{12}^{(1)}+4\tau_p}{2\,(2+m)}, \\
\gamma_{12}^{(3)} &= \frac{\gamma_{12}^{(2)}-2\tau_p+\beta_{ap\,1}\gamma_{12}^{(2)}+\beta_{ap\,2}\gamma_{12}^{(1)}}{(3+m)}, \\
\gamma_{12}^{(4)} &= \frac{3\gamma_{12}^{(3)}+\tau_p+2\beta_{ap\,1}\gamma_{12}^{(3)}+2\beta_{ap\,2}\gamma_{12}^{(2)}+2\beta_{ap\,3}\gamma_{12}^{(1)}}{2\,(4+m)},
\end{aligned}$$

$$\begin{aligned}
\gamma_{21}^{(1)} &= \frac{1}{1+m}, \\
\gamma_{21}^{(2)} &= -\frac{\gamma_{21}^{(1)}-1+2\beta_{rp\,1}\gamma_{21}^{(1)}}{2\,(2+m)}, \\
\gamma_{21}^{(3)} &= -\frac{\gamma_{21}^{(2)}+\beta_{rp\,1}\gamma_{21}^{(2)}+\beta_{rp\,2}\gamma_{21}^{(1)}}{(3+m)}, \\
\gamma_{21}^{(4)} &= -\frac{3\gamma_{21}^{(3)}+2\beta_{rp\,1}\gamma_{21}^{(3)}+2\beta_{rp\,2}\gamma_{21}^{(2)}+2\beta_{rp\,3}\gamma_{21}^{(1)}}{2\,(4+m)},
\end{aligned}$$

[1]Note that the series in (36) are absolutely convergent within the intervals defined as above by constants $\mathcal{K}_{ij}=\max\left\{\sqrt[k]{\left|\gamma_{1j}^{(k)}\right|},\ k=1,2,3,4,5\right\}$.

$$
\begin{aligned}
\gamma_{22}^{(1)} &= -\frac{(1-\tau_p)(\xi_f^2-1)}{1+m}, \\
\gamma_{22}^{(2)} &= -\frac{\gamma_{21}^{(1)}+(1-\tau_p)(\xi_f^2-1)+2\beta_{rp\,1}\gamma_{21}^{(1)}+4\tau_p}{2\,(2+m)}, \\
\gamma_{22}^{(3)} &= -\frac{\gamma_{22}^{(2)}+2\tau_p+\beta_{rp\,1}\gamma_{22}^{(2)}+\beta_{rp\,2}\gamma_{22}^{(1)}}{(3+m)}, \\
\gamma_{22}^{(4)} &= -\frac{3\gamma_{22}^{(3)}+\tau_p+2\beta_{rp\,3}\gamma_{22}^{(1)}+2\beta_{rp\,2}\gamma_{22}^{(2)}+2\beta_{rp\,1}\gamma_{22}^{(3)}}{2\,(4+m)},
\end{aligned}
$$

and, for $j=1,2$,

$$
\gamma_{1j}^{(k)} = \frac{(k-1)\gamma_{1j}^{(k-1)}+2\sum_{s=1}^{k-1}\beta_{ap\,s}\gamma_{1j}^{(k-s)}}{2\,(k+m)},\ k=5,6,\dots\ , \tag{37}
$$

$$
\gamma_{2j}^{(k)} = -\frac{(k-1)\gamma_{2j}^{(k-1)}+2\sum_{s=1}^{k-1}\beta_{rp\,s}\gamma_{2j}^{(k-s)}}{2\,(k+m)},\ k=5,6,\dots\ . \tag{38}
$$

6. Abramov method for WGM calculations

The numerical integration of the system of equations (26), (27), (29) can be performed using any standard algorithm. For instance, the results presented in Tables 1 and 2 were computed using the classical 4-th order Runge-Kutta method combined with an adaptive step-size routine. Note that the integration of the system (26), (27), (29) is stable only in the direction away from the singular point [1, 2].

In [3, 4], it was stated and proved for regular ODEs that the method works dependably regardless of the 'freezing points'. However, in our case, due to the singularity, this does not hold: by moving the 'freezing points' towards the singular points, the difference in starting values $\lambda_0=\lambda_f$ and $c^2=c_f^2$, can be arbitrary large, see Eq. (15). This means that the constant C defined at the end of Section 4 strongly depends on the choice of the 'freezing point' (η_f,ξ_f).

In Table 1, the dependence of both, the initial guess and the calculated eigenvalues on the 'freezing point' is presented. The calculations were performed for two marching stepsizes: $h_\tau=10^{-3}$ and $h_\tau=10^{-4}$ and a uniform τ-grid.

η_f,	ξ_f	λ_f,	c_f^2	λ_P, c_P^2 $P=1000$		λ_P, c_P^2 $P=10000$	
0.99	1.04	8019.746	104540.294	9646.963	455.257	9649.494	452.712
0.95	1.2	8175.341	19741.097	9648.052	454.162	9649.626	452.580
0.75	2.0	8749.627	3086.790	9337.598	452.666	9649.785	452.420
0.5	3.0	9190.597	1212.667	9649.726	452.431	9649.809	452.396
0.25	4.0	9475.931	665.778	9649.810	452.395	9649.813	452.392
0.05	4.8	9640.659	460.590	9649.813	452.392	9649.813	452.392

Table 1: Dependence of the initial guess and the calculated eigenvalues on the 'freezing point' (η_f,ξ_f): Neumann boundary conditions, $\xi_s=5.0$, $m=100$, $n=l=0$. Correct values are $\lambda=9649.81290$ and $c^2=452.39201$.

As we can see from Table 1, the successful numerical integration of Eqs. (26)–(27) is hindered by the fact that the values of the Newton iterates for the spectral parameters, λ_p, c_p^2 may become very large, especially due to the un-suitable choice of the 'freezing point', and so the right-hand sides of these equations. Moreover, in WGM calculations we have to

deal with the angular momentum number $m \sim 1000$, which makes the right hand sides of Eqs. (26), (27) huge, especially near singularities regardless of the 'freezing point' choice.

As a consequence, due to the steep 'staircase' behaviour, the accurate calculation of the Prüfer angles from Eqs. (26), (27) becomes difficult (see, e.g., [21]). In particular, this explains why the Prüfer angle is rarely used in numerical methods, despite of its previously mentioned attractive properties. In [1, 2, 21] a modification of the Prüfer angle is invented, making the modified Prüfer angle less steep. The modification takes into account the classical WKB approximations for second order ODE solutions [15]. The modified Prüfer angle $\theta_{mod}(\cdot)$ relates to the classical one as

$$\tan\theta = \nu \tan\theta_{mod},$$

where the 'scaling function' $\nu(\cdot)$ compensates for the sharp change of the Prüfer angle. Due to Eq. (26), the best choice of $\nu(\eta)$ at the points where $|Q_a(\eta)| \gg 0$ would be $\nu(\eta) = \sqrt{|(1-\eta^2)Q_a(\eta)|}$. Similarly, for the radial part the optimal scaling should be $\nu(\xi) = \sqrt{|(\xi^2-1)Q_r(\xi)|}$, if $|Q_r(\xi)| \gg 0$. However, a very primitive scaling $\nu = \sqrt{m^2+1}$ allows to accurately integrate both equations (26) and (27) even in such extreme cases as presented in Table 2.

In all calculations presented in Table 2 the accuracy of the integration of the auxiliary functions $\theta_{a,r}$, as well as the Jacobi matrix entries k_{ij} was $\varepsilon = 10^{-5}$. Note that the error ε_N caused by the truncation of the series (31), (32) and (36) was therewith taken into account. Calculations were performed for the Neumann boundary condition imposed on the surface of spheroid $\mathcal{S}$. The 'freezing points' were $\eta_f = 0.01$ and $\xi_f = 1.99$. The number of marching steps was sufficiently large for the couples $(\lambda_{ln\,P}, c^2_{ln\,P})$ to satisfy equalities (12) in the P-th step with the desired accuracy ε. Moreover, the Newton iterations were continued at $p = P$, i.e. $\tau = 1$ until the resulting values stabilized at (λ_{ln}, c^2_{ln}).

multi–index			Resonator	Step number	Eigenvalue			
m	l	n	ξ_s	P	$\lambda_{ln\,P}$	$c^2_{ln\,P}$	λ_{ln}	c^2_{ln}
1000	0	0	100.0	10000	1000898.3205	101.7302	1000898.3205	101.7302
2000	0	0	50.0	2000	4000382.6393	1617.7643	4000382.6393	1617.7643
2000	5	5	10.0	2000	3977964.7164	44185.9632	3977964.7164	44185.9632
5000	0	0	10.0	2000	24751052.4085	253972.9170	24751052.4086	253972.9169
2000	50	50	2.0	2000	2247327.3126	2001396.5973	2247326.9339	2001396.9873
3000	0	0	2.0	1000	5979249.5015	3024217.9051	5979249.5017	3024217.9049
5000	0	0	2.0	2000	16624872.6782	8380904.7533	16624872.6797	8380904.7529
10000	0	0	2.0	10000	66559133.0900	33452418.8827	66559133.0905	33452418.8821
2000	0	0	1.1	1000	-15241365.7692	19246186.5779	-15241365.7692	19246186.5779
3000	0	0	1.1	1000	-34189787.2511	43197011.3801	-34189787.2511	43197011.3801
1000	100	100	1.1	2000	-10363422.4943	12086667.7479	-10363422.4940	12086667.8244

Table 2: Eigenvalue calculations with the modified Abramov method.

In general, since the constant C in the error estimate is not known *a priori*, as well as the number P of marching steps that guarantees the desired accuracy of the resulting values λ_P, c^2_P, we recommend to repeat calculations at each (or certain) marching step τ_p until the criterion (12) is satisfied within the prescribed accuracy.

Therewith the intermediate values λ_p and c^2_p will approach the exact eigenvalues $\lambda(\tau_p)$, $c^2(\tau_p)$ that lay on the curve $\lambda = \lambda(\tau)$, $c^2 = c^2(\tau)$ connecting the eigenvalues of the 'frozen' and original problems.

The existence of such a curve opens other possibilities for the application of the Newton method combined with the time-parameter marching. One of them converts the original Sturm–Liouville problem into the algebraic problem via a discretization based on the high order finite difference (HOFiD) schemes [7, 8, 9, 10, 11].

7. Finite difference schemes

The HOFiD method is based on the idea to approximate each derivative separately by using high order finite difference schemes, see [7, 8, 9, 10, 11] for details. In brief, the

original continuous problem is transformed into a discrete system of equations where the unknowns are approximations of the solution in given points of the integration interval. The derivatives in the continuous problem are approximated with linear combinations obtained by finite differences. In the following, let A_ι for $\iota = 1, 2$, be the banded matrix of the coefficients approximating, respectively, the first and the second derivative [10] for any considered discretization.

In this section, we solve equations (1)-(2), where again due to the symmetry, we consider only half of the integration interval for S. We combine the Abramov approach described in Section 4 with the HOFiD method (see [8, 9]), that is, we discretize the Sturm-Liouville problem as well as all the 'intermediate' p-th problems where equations (1) and (2) are replaced with (18) and (19).

In [5, 6] HOFiD_MSP needs initial approximations of the eigenvalues given by the Prüfer angle technique in order to compute a very precise approximation of both eigenvalues and eigenfunctions. Now, following the idea outlined in Section 4, we just deal with these initial approximations which enables HOFiD_MSP package to compute automatically eigenparameters and eigenfunctions corresponding to fixed (l, n) (see also [12]). To this aim, we define a set of problems depending on the quasi-time parameter $\tau_p \in [0, 1]$. We start with $\tau_0 = 0$ discretizing the 'frozen problem' (13)–(14) at an arbitrary point (η_f, ξ_f) in order to obtain two uncoupled discrete problems

$$\begin{cases} S_{0,0} = 0 \quad \text{or} \quad A_1^{(1)} S_0 = 0, \\ (1 - \eta_{N_\eta}^2) A_1^{(N_\eta)} S_0 = \beta_a(\eta_{N_\eta}) S_{0,N_\eta}, \\ (I - D_\eta^2) A_2 - 2 D_\eta A_1 + [\mu I - m^2 (I - D_\eta^2)^{-1}] S_0 = 0, \\ h_\eta S_0^T D_1 S_0 = 0, \end{cases} \tag{39}$$

and

$$\begin{cases} R_{0,N_\xi} = 0 \quad \text{or} \quad A_1^{(N_\xi)} R_0 = 0, \\ (\xi_0^2 - 1) A_1^{(1)} R_0 = \beta_r(\xi_0) R_{0,0}, \\ (D_\xi^2 - I) A_2 + 2 D_\xi A_1 + [\nu I - m^2 (D_\xi^2 - I)^{-1}] R_0 = 0, \\ h_\xi R_0^T D_2 R_0 = 0, \end{cases} \tag{40}$$

where we subdivide the two integration domains with N_η and N_ξ equispaced intervals having stepsizes h_η and h_ξ, respectively. S_0 and R_0 contain the unknown discrete approximations of the eigenfunctions $S_{0,i} \approx S_0(\eta_i)$ $(i = 0, \ldots, N_\eta)$, and $R_{0,i} \approx R_0(\xi_i)$ $(i = 0, \ldots, N_\xi)$, the diagonal matrices D_x contain the values $x_0, \ldots, x_{N_x}$, for $x = \eta, \xi$, D_1 and D_2 are diagonal matrices resulting from the quadrature formulae approximating the normalization conditions.

This problem has been already solved by using an algebraic approach in which we compute the eigenvalues and eigenvectors of banded matrix [8] or by standard techniques for the nonlinear systems [11].

Starting with (λ_0, c_0^2) and the corresponding eigenfunctions S_0, R_0, we now solve the

problem (18)–(19) by means of the following discrete problems

$$\begin{cases} S_{p,0} = 0 \text{ or } A_1^{(1)} S_p = 0 \quad \text{and} \quad R_{p,N_\xi} = 0 \text{ or } A_1^{(N_\xi)} R_p = 0, \\ (1-\eta_{N_\eta}^2) A_1^{(N_\eta)} S_p = \beta_a(\eta_{N_\eta}) S_{p,N}, \qquad (\xi_0^2 - 1) A_1^{(1)} R_p = \beta_r(\xi_0) R_{p,0}, \\ (I - D_\eta^2) A_2 - 2 D_\eta A_1 + [\lambda I + c^2 V_{p,\eta} - m^2 (I - D_\eta^2)^{-1})] S_p = 0, \\ (D_\xi^2 - I) A_2 + 2 D_\xi A_1 + [c^2 W_{p,\xi} - \lambda I - m^2 (D_\xi^2 - I)^{-1})] R_p = 0, \\ h_\eta S_p^T D_1 S_p = 0, \qquad h_\xi R_p^T D_2 R_p = 0, \end{cases} \tag{41}$$

where $V_{p,\eta} = \tau_p (I - D_\eta^2) + (1-\tau_p)(1-\eta_f^2) I$ and $W_{p,\xi} = \tau_p (D_\xi^2 - I) + (1-\tau_p)(\xi_f^2 - 1) I$, with τ_p strictly increasing values in $[0,1]$, $p = 0, \ldots, P$ (in contrast to (17)). Note that, since each problem (41) has more solutions corresponding to different oscillations of the eigenfunctions, an approximation of the eigenparameters $(\lambda_{p-1}, c_{p-1}^2)$ obtained for τ_{p-1} needs to be used as an initial guess for the next step τ_p in the calculation of (λ_p, c_p^2). Moreover, since the HOFiD method also gives an approximation of the eigenfunctions, to improve the convergence of the nonlinear problem (41), the approximations S_{p-1}, R_{p-1} obtained for τ_{p-1} are used as initial guess for S_p, R_p in τ_p.

Solutions of the original problem (1) and (2) are obtained in the last step for $\tau_P = 1$. By choosing appropriately the numbers N_η, N_ξ and P it is possible to compute the intermediate eigenvalues on the spectral curve connecting the frozen and the true eigenvalues. The number of oscillations of the eigenfunctions are used to verify that the proper eigenparameters are computed.

8. Numerical simulations with HOFID_MSP

In this section, we discuss the performance of the HOFiD_MSP code carrying out the approach presented in the previous section for the parameters m, l, k in the range of interest. We are interested in the computation of an approximation of the solution with few correct significant digits since, to compute a more accurate solution, we have already developed the code HOFiD_MSP with variable stepsize (see [5, 6]). Here, this latter code, which requires as input an initial approximation of the eigenparameters, is only used to estimate the approximation error in Table 3.

For the discretization of the problem we use constant stepsizes. Moreover, we use equispaced values for τ_p. For what concerns the transferred boundary conditions in Section 5, in the calculations below the parameters δ_η and δ_ξ were set to 10^{-4}.

We observe beforehand that the choice of (η_f, ξ_f) identifying the 'frozen problem' is not very important for the HOFiD_MSP code that uses the marching step to move from the intermediate problem to the original one. In Fig. 1, we show the paths to calculate the eigenparameters with $(l, n) = (0, 1)$ using different starting points (η_f, ξ_f). We emphasize that, even if the distance between the freezing eigenvalues and the exact ones depends on (η_f, ξ_f), the number of steps required to reach the estimation of the final eigenparameters $(\lambda_P,\, c_P)$ is unchanged for the considered example. The only requirement is that eigenvectors are computed with a sufficient accuracy in order to guarantee that the number of oscillations remains unchanged.

In the next experiments, $\xi_s = 5$ and the parameters (η_f, ξ_f) are $(0.5, 3)$. The important feature of the underlying problem is that lines (from $\tau_0 = 0$ to $\tau_P = 1$) corresponding to different eigenparameters do not intersect (see Fig. 2). This prevents the numerical approximations to jump from one spectral curve to another.

In Table 3 we show the relative error for λ and c^2 obtained for different boundary conditions, large azimuthal number m and small numbers of oscillations l and n. We have

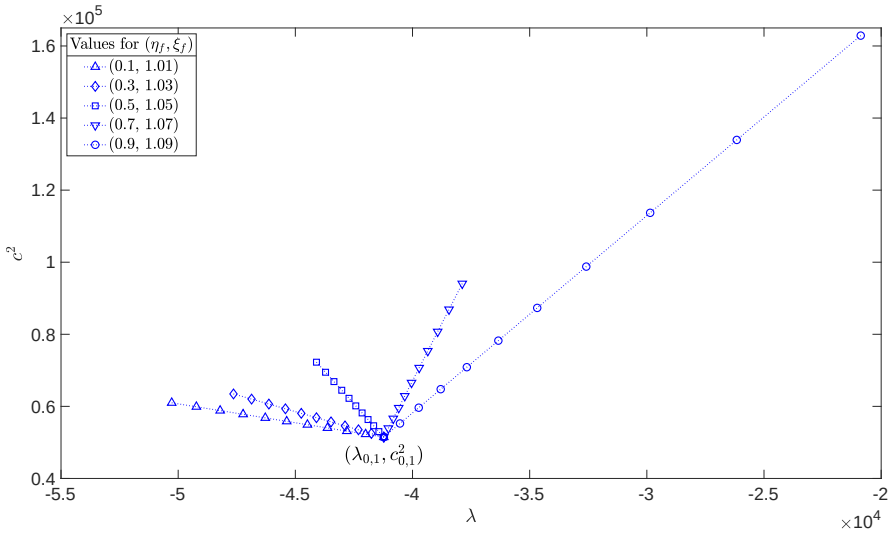

Figure 1: Prolate problem with $m = 100$, $\xi_s = 1.1$ and $S'(0) = R'(\xi_s) = 0$ solved with $N_\eta = N_\xi = 50$. Path for the eigenparameters estimation with $(l, n) = (0, 1)$ for τ_p running from $\tau = 0$ to $\tau = 1$ with $P = 10$ steps and different choices of the starting point (η_f, ξ_f).

chosen order 6 formulae and stop criterion for the Newton iteration equal to 10^{-3}. The results in Table 3 show that for a successful code run, we require fine discretizations and large values of P especially when l and/or n are large. The value of P can be reduced by using an automatic variable mesh for $\tau_p \in [0,\ 1]$ (see [12]). However, at this stage we are only interested in the existence of a minimum number P (with equispaced τ_p values) that guarantees the existence of a convergent marching path.

							HOFiD_MSP		
	m	l	n	ξ_s	λ	c^2	(P, N_η, N_ξ)	Error λ	Error c^2
$R'(\xi_s)=0$	1000	0	0	1.1	-3838829.69823	4841245.94361	(10, 50, 50)	1.41e-3	8.71e-4
	1000	0	10	5.0	949772.40666	51252.86305	(1000, 100, 400)	3.21e-5	7.74e-4
	5000	0	0	5.0	23957468.33103	1047635.32721	(20, 200, 200)	6.17e-5	1.48e-3
	5000	2	0	1.1	-94696609.22667	119756764.61349	(20, 300, 300)	3.56e-4	2.70e-4
	10000	4	2	5.0	95852388.63741	4239518.09321	(100, 1000, 1000)	1.60e-6	3.65e-5
$R(\xi_s)=0$	1000	0	1	1.1	-4078620.81814	5081086.17732	(10, 50, 100)	2.25e-3	1.57e-3
	5000	10	5	5.0	24009254.37073	1098129.96394	(100, 600, 600)	7.32e-5	1.63e-3
	5000	20	10	1.1	-103078345.84109	128586350.72766	(20, 900, 900)	1.24e-5	3.78e-6
	10000	0	0	5.0	95809706.46358	4200501.37087	(20, 300, 300)	5.71e-5	1.28e-3
	10000	10	0	1.1	-379922978.84256	480428885.58569	(20, 600, 600)	9.84e-6	6.13e-5

Table 3: Eigenvalue calculations for the prolate problem with the HOFiD_MSP code and their relative errors.

In this table the reference values of the eigenvalues (in order to compute the errors) have been obtained by means of the HOFID_MSP code with variable stepsize by using 10^{-12} exit tolerance.

As an illustration of the above calculations, the WGM mode inside the spheroid with $\xi_s = 1.1$ is shown in Fig. 3 (left plot). It corresponds to the azimuthal number $m = 5000$, while $l = 6$ and $n = 4$. The turquoise colour corresponds to the unperturbed region of the spheroid, and we can see that the perturbation is concentrated around its equator. Such an unusual behaviour is a consequence of the particular form of the separated eigenfunction components $S_{6,4}(\eta)$ and $R_{6,4}(\xi)$ (right plots). The latter is explained by the position of the turning points of Eqs. (1), (2), i.e. the values η_{tp}, ξ_{tp}, where the functions $Q_a(\eta, \lambda, c^2)$, $Q_r(\xi, \lambda, c^2)$ change their signs.

Thus, for the eigenvalue $(\lambda_{6,4}, c^2_{6,4}) = (-98862013.0533, 124020698.2469)$, the function

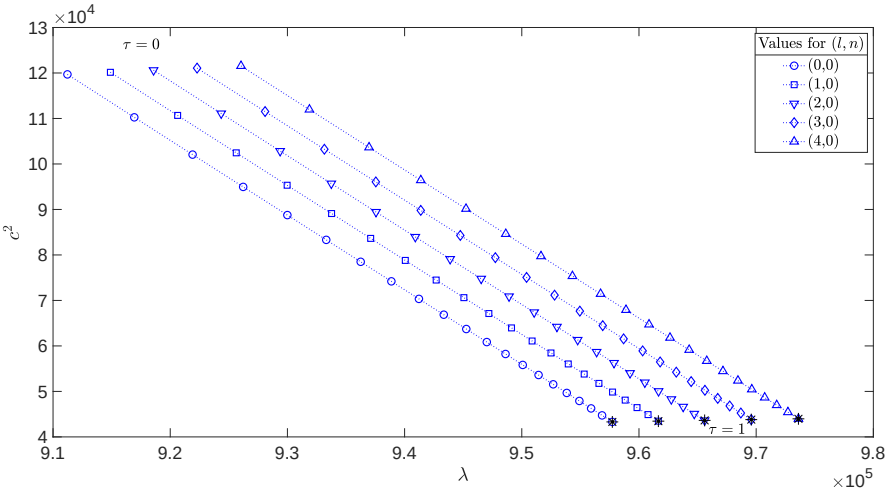

Figure 2: Prolate problem with $m = 1000$, $\xi_s = 5$ and $S'(0) = R(\xi_s) = 0$ solved with $N_\eta = N_\xi = 150$. Path from $\tau = 0$ to $\tau = 1$ for the eigenparameters estimation with $(l, n) = (0, 0), \ldots, (4, 0)$. The final eigenparameters $(\lambda_{l,n,P}, c_{l,n,P})$ are marked with $*$.

$Q_a(\eta, \lambda, c^2)$ is positive within the subinterval $(-\eta_{tp}, \eta_{tp})$ with $\eta_{tp} = 0.0326$, and hence solutions of Eq. (1) oscillate inside this subinterval, exponentially decaying outside of it. Similarly, $Q_r(\xi, \lambda, c^2) > 0$ for $\xi_{tp} < \xi < \xi_s$, where $\xi_{tp} = 1.0963$. Hence, solutions of the radial equation (2) oscillate inside (ξ_{tp}, ξ_s) and exhibit an exponential behaviour on $(1, \xi_{tp})$, where $Q_r(\xi, \lambda, c^2)$ is negative.

9. Conclusions

In this paper, we discussed the Abramov approach for the numerical simulation of the whispering gallery modes in prolate spheroids. In the first step, a solution of a simpler problem, as an initial guess for the Newton-Raphson iteration, is provided. Then, gradually, this simpler problem is converted into the original problem, while the quasi-time parameter τ runs from $\tau = 0$ to $\tau = 1$. In other words, we are following an imaginary path leading from a simpler problem formulation to the original one. Two numerical approaches are realized, the first is based on the Prüfer angle technique, the second on the high order finite difference schemes.

More precisely, the coefficients near eigenvalue components λ and c^2 are 'frozen' at an arbitrary point $(\eta_f, \xi_f) \in (0, 1) \times (1, \xi_s)$, consequently defining the so-called 'frozen' problem (13)–(14) which formally is a two–parameter problem, but each equation can be treated independently with respect to the eigenparameters $\mu = \lambda + c^2(1 - \eta_f^2)$ and $\nu = c^2(\xi_f^2 - 1) - \lambda$.

The run of the quasi-time parameter τ in the interval $[0, 1]$ allows a gradual transition from the problem (13)–(14) with 'frozen' coefficients to the original problem defined by (1)–(2).

It turned out that, in the first attempts to use Abramov's method, not all his expectations [3, 4] have been satisfied. To begin with, the role of the 'freezing point' was underestimated. Since the ratio $\frac{1}{\xi_f^2 - \eta_f^2}$ in Eq. (15), and hence the distance between the starting guess (λ_f, c_f^2) and the exact eigenvalue (λ, c^2), can be made as large as desired, the performance of the method strongly depends on the chosen 'freezing point' (η_f, ξ_f). Although a finite number of marching steps was shown to approximate the solution up to any prescribed accuracy, a strict accuracy requirement may result in a very fine step size in the marching parameter τ.

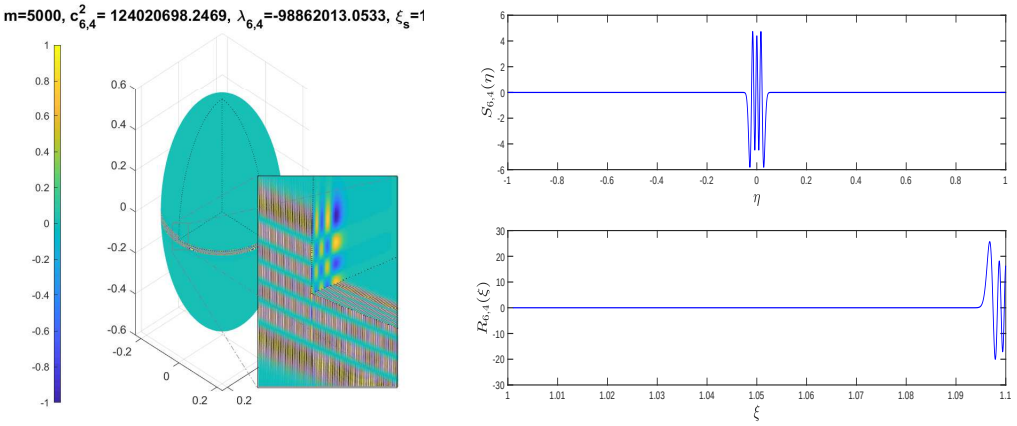

Figure 3: Left: WGM mode $m = 5000$, $l = 6$, $n = 4$ in the ellipsoid with $\xi_s = 1.1$. Right: the related angular component $S_{6,4}(\eta)$ (upper plot) and radial component $R_{6,4}(\xi)$ (lower plot). On the surface of the spheroid a Neumann boundary condition for R is imposed.

Furthermore, due to the singularity of the problem, the boundary conditions have to be moved from the singular point to a close regular point to make the Abramov technique applicable. Moreover, the solutions of the auxiliary ODEs may have very steep gradients, unless an appropriate scaling is found.

Nevertheless, after an appropriate modification, our method managed to perform calculations of the eigenoscillations inside prolate spheroids of various eccentricities, from almost a sphere to a very prolate 'cigar'. In particular, we were able to calculate highly localized WGMs inside a prolate spheroid, which are important in many scientific and industrial applications in the context of optics and photonics [14, 22, 23, 24, 31]. Moreover, adopting Abramov's idea of parameter marching along the spectral curve and connecting the eigenvalues of the frozen and original problems, we designed an additional powerful algorithm for solving the problem (1)–(4) based on high order finite difference schemes.

The estimation of the run-times and storage demand for the involved algorithms is difficult. However, the qualitative comparison of the Prüfer angle approach and high order finite difference schemes is possible. The Prüfer angle method calculations involve numerical integration of a system of six first order ODEs and inversion of a small 2×2 matrix, while the high order finite difference schemes imply inversion of a large but easy to compute matrix. We emphasize that the considered algorithms work automatically.

The HOFiD_MSP code computes both the eigenparameters and the eigenfunctions with a desired number of oscillations. For the computation of the eigenfunctions and various functionals depending on them with the help of the Prüfer function we refer the reader to [1, 21].

Note that the above spectral curve (connecting the eigenvalues of the frozen and original problems) does not depend on the particular numerical recipe and may be 'marched over' using any other algebraic formulation of the Sturm-Liouville problem (1)–(4).

The presented efficient and reliable numerical technique is applicable not only to simulate the prolate spheroids, but can be also used for the investigation of a wide spectrum of internal boundary value problems arising inside resonator cavities of all separable geometries.

Acknowledgements

The authors gratefully acknowledge the warm hospitality of Vienna University of Technology, Vienna, Austria. The second author (A.A.) was partially supported by the bi-

national FWF-project I3538-N32.

References

[1] Abramov et al., Computation of Prolate Spheroidal Functions by Solving the Corresponding Differential Equations, *Comput. Math. Math. Phys.* **24** (1984), 1–11.

[2] A.A. Abramov, A.L. Dyshko, N.B. Konyukhova, and T.V. Levitina, Evaluation of Lamé Angular wave functions by solving of auxiliary differential equations, *Comput. Math. Math. Phys.* **29** (1989), 119–131.

[3] A.A. Abramov and V.I. Ulyanova, A method for solving selfadjoint multiparameter spectral problems for weakly coupled sets of ordinary differential equations, *Comput. Math. Math. Phys.* **37:5** (1997), 552–557.

[4] A.A. Abramov and V.I. Ulyanova, A method for solving self-adjoint multiparameter spectral problems for systems of equations with singularities, *Comput. Math. Math. Phys.* **38:10** (1998), 1566–1570.

[5] P. Amodio, T. Levitina, G. Settanni, and E. B. Weinmüller, Numerical simulation of the whispering gallery modes in prolate spheroids, *Comput. Phys. Commun.* **185** (2014), 1200–1206.

[6] P. Amodio, T. Levitina, G. Settanni, and E. B. Weinmüller, Whispering gallery modes in oblate spheroidal cavities: Calculations with a variable stepsize, *Numerical Analysis and Applied Mathematics, AIP Conf. Proc.* **1648** (2015), 150019.

[7] P. Amodio, T. Levitina, G. Settanni, and E. B. Weinmüller, On the Calculation of the Finite Hankel Transform Eigenfunctions, *J. Appl. Math. & Computing* **43** (2013), 151–173.

[8] P. Amodio and G. Settanni, A matrix method for the solution of Sturm-Liouville problems, *JNAIAM J. Numer. Anal. Indust. Appl. Math.* **6** (2011), 1–13.

[9] P. Amodio and G. Settanni, A stepsize variation strategy for the solution of regular Sturm-Liouville problems, *Numerical Analysis and Applied Mathematics, AIP Conf. Proc.* **1389** (2011), 1335-1338.

[10] P. Amodio and G. Settanni, A finite differences MATLAB code for the numerical solution of second order singular perturbation problems, *Journal of Computational and Applied Mathematics* **236** (2012), 3869–3879.

[11] P. Amodio and G. Settanni, Variable-step finite difference schemes for the solution of Sturm-Liouville problems, *Commun. Nonlinear. Sci. Numer. Simulat.* **20** (2015), 641–649.

[12] P. Amodio and G. Settanni, Numerical Strategies for Solving multiparameter Spectral Problems, in: *NUMTA 2019: Numerical Computations: Theory and Algorithms (Y.D. Sergeyev, D.E. Kvasov editors), Lecture Notes in Computer Science* **11974**, part II (2020), 298–305.

[13] T. Bhattacharyya, H. Binding and P.A. Seddighi, Multiparameter Sturm-Liouville problems with eigenparameter dependent boundary conditions, *Journal of Mathematical Analysis and Applications* **264:2** (2001), 560–576.

[14] L. Cai, J. Pan and S. Hu, Overview of the coupling methods used in whispering gallery mode resonator systems for sensing, *Optics and Lasers in Engineering* **127** (2020), art. no. 105968.

[15] N. Fröman and P. O. Fröman, *JWBK-approximation*, North-Holland (1965).

[16] M.L. Gorodetsky and V.S. Ilchenko, High-Q optical whispering gallery microresonators: Precession approach for spherical mode analysis and emission patterns with prism couplers, *Opt. Comm.* **113** (1994), 133–143.

[17] V.S. Ilchenko and A.B. Matsko, Optical resonators with whispering gallery nodes — Part II: Applications, *IEEE J. Sel. Topics Quantum Electron.* **12** (2006), 15–32.

[18] I.V. Komarov, L.I. Ponomarev, and S.Yu. Slavyanov, *Spheroidal and Coulomb Spheroidal Functions*, (in Russian), Nauka, Moscow, 1976.

[19] T.V. Levitina, The conditions of applicability of an algorithm for solving two-parameter self-adjoint boundary-value problems, *Zh. Vychisl. Mat. Mat. Fiz.* **31:5** (1991), 689–697.

[20] T.V. Levitina, A numerical solution to some three-parameter spectral problems, *Zh. Vychisl. Mat. Mat. Fiz.* **39:11** (1999), 1787–1801.

[21] T.V. Levitina and E.J. Brändas, Computational techniques for Prolate Spheroidal Wave Functions in Signal Processing, *J. Comp. Meth. Sci. & Engrg.* **1** (2001), 287–313.

[22] M.-T. Li, Z.-S. Hou, Q.-L. Huang, S. Xu and A.-W. Li, Laser printing controllable photonic-molecule microcavities *Optics Communications* **459** (2020), art. no. 125036.

[23] A.B. Matsko and V.S. Ilchenko, Optical resonators with whispering gallery nodes — Part I: basics, *IEEE J. Sel. Topics Quantum Electron.* **12** (2006), 3–14.

[24] A.B. Matsko, A.A. Savchenkov, D. Strekalov, V.S. Ilchenko, and L. Maleki, Review of Applications of Whispering-Gallery Mode Resonators in Photonics and Nonlinear Optics, *IPN PR – Nasa* **42-162** (2005), 1–51.

[25] P.M. Morse and H. Feshbach, *Methods of Theoretical Physics*, McGrawHill, New York, 1953.

[26] B.D. Sleeman, *Multiparameter Spectral Theory in Hilbert Space*, Research Notes in Mathematics, vol. 22, Pitman, London, 1978.

[27] B.D. Sleeman, Multiparameter spectral theory and separation of variables, *J.* Phys. A: Mathematical Theory **41** (2008), 1–20.

[28] H. Volkmer, Multiparameter Eigenvalue Problems and Expansion Theorems, *Lecture Notes in Mathematics* **1356**, Springer-Verlag, Berlin, New York, 1988.

[29] L. Weinstein, *Open Resonators and Open Waveguides*, The Golem Press, Boulder, Colorado, 1969.

[30] https://en.wikipedia.org/wiki/Whispering_gallery, February 24th 2020.

[31] G. Zhu, J. Li, N. Zhang, X. Li, J. Dai, Q. Cui, Q. Song, C. Xu and Y. Wang, Whispering-Gallery Mode Lasing in a Floating GaN Microdisk with a Vertical Slit (2020) *Scientific Reports* **10** (1) (2020), art. no. 253.